

Mitochondrial oxodicarboxylate carrier deficiency is associated with mitochondrial DNA depletion and spinal muscular atrophy-like disease

Veronika Boczonadi PhD^{1*}, Martin S. King PhD^{2*}, Anthony C. Smith PhD², Monika Olahova PhD³, Boglarka Bansagi MD¹, Andreas Roos PhD^{1,4}, Filmon Eyassu PhD², Christoph Borchers PhD⁵, Venkateswaran Ramesh MD⁶, Hanns Lochmüller MD¹, Tuomo Polvikoski MD⁷, Roger G. Whittaker MD⁸, Angela Pyle PhD¹, Helen Griffin PhD¹, Robert W. Taylor PhD³, Patrick F. Chinnery FRCP, FMedSci^{2,9}, Alan J. Robinson PhD², Edmund R.S. Kunji PhD^{2*}, Rita Horvath MD, PhD^{1*}

¹Wellcome Centre for Mitochondrial Research, Institute of Genetic Medicine, Newcastle University, Newcastle upon Tyne, UK;

²Medical Research Council Mitochondrial Biology Unit, University of Cambridge, Cambridge Biomedical Campus, Wellcome Trust / MRC Building, Hills Road, Cambridge, CB2 0XY, UK;

³Wellcome Centre for Mitochondrial Research, Institute of Neuroscience, Newcastle University, Newcastle upon Tyne, UK;

⁴Leibniz Institute of Analytic Sciences (ISAS), Dortmund, Germany;

⁵UVic-Genome BC Proteomics Centre, Vancouver, Canada;

⁶Department of Paediatric Neurology, Royal Victoria Infirmary, Newcastle upon Tyne Foundation Hospitals NHS Trust, Newcastle upon Tyne, UK;

⁷Institute for Ageing and Health, Newcastle University, Newcastle upon Tyne, UK;

⁸Institute of Neuroscience, Newcastle University, Newcastle upon Tyne, UK;

⁹Department of Clinical Neurosciences, University of Cambridge, Cambridge Biomedical Campus, Cambridge, CB2 0QQ, UK

*VB and MSK contributed equally to this study

*ERSK and RH contributed equally to this study

Word count: 3901 words

Abstract: 200 words

Title: 137 characters

Running title: Mitochondrial oxodicarboxylate carrier deficiency

Corresponding authors:

Rita Horvath, MD PhD, Institute of Genetic Medicine, Newcastle University, Central Parkway, NE1 3BZ, Newcastle upon Tyne, UK

Tel: +44 (0)191 2418855, Fax: +44 (0)191 2418855, Email: rita.horvath@ncl.ac.uk

Edmund R.S. Kunji, PhD, Medical Research Council Mitochondrial Biology Unit, University of Cambridge, Wellcome Trust / MRC Building, Cambridge Biomedical Campus, Hills Road, Cambridge, CB2 0XY, United Kingdom

Phone: Tel.: +44 (0)1223 252850, Email: ek@mrc-mbu.cam.ac.uk

ABSTRACT

Purpose: Members of the mitochondrial carrier family (SLC25) transport metabolites, nucleotides, co-factors and inorganic ions across the mitochondrial inner membrane.

Methods: We identified a pathogenic variant in a novel mitochondrial carrier gene in a patient by whole exome sequencing. The pathogenicity of the mutation was studied by transport assays, computer modelling followed by targeted metabolic testing and *in vitro* studies in human fibroblasts and neurons.

Results: The patient carries a homozygous pathogenic variant c.695A>G; p.(Lys232Arg) in the *SLC25A21* gene, encoding the mitochondrial oxodicarboxylate carrier, and developed spinal muscular atrophy and mitochondrial myopathy. Transport assays show that the mutation renders SLC25A21 dysfunctional and 2-oxoadipate cannot be imported into the mitochondrial matrix. Computer models of central metabolism predicted that impaired transport of oxodicarboxylate disrupts the pathways of lysine and tryptophan degradation, and causes accumulation of 2-oxoadipate, pipercolic acid and quinolinic acid, which was confirmed in the patient's urine by targeted metabolomics. Exposure to 2-oxoadipate and quinolinic acid decreased the level of mitochondrial complexes in neuronal cells (SH-SY5Y) and induced apoptosis.

Conclusion: Mitochondrial oxodicarboxylate carrier deficiency leads to mitochondrial dysfunction and the accumulation of oxoadipate and quinolinic acid, which in turn cause toxicity in spinal motor neurons leading to spinal muscular atrophy-like disease.

Key words: metabolite transport, spinal motor atrophy, mitochondrial respiratory chain deficiency, neural toxicity, metabolomics.

Abbreviations: SLC25A21 mitochondrial oxodicarboxylate carrier; FVC forced vital capacity; SMA spinal muscular atrophy; CK creatine kinase; CSF cerebrospinal fluid; COX cytochrome *c* oxidase; mtDNA mitochondrial DNA.

INTRODUCTION

Several inherited diseases with very variable clinical presentations are associated with dysfunctional mitochondrial carriers (SLC25), which transport nucleotides, keto acids, amino acids, fatty acids, co-factors and inorganic ions across the mitochondrial inner membrane¹⁻⁵. They cause various metabolic syndromes often affecting skeletal muscle (e.g. rhabdomyolysis, lipid storage myopathy, and neuromuscular transmission), heart (cardiomyopathy) or the nervous system (e.g. neuropathy, neonatal epileptic encephalopathy, and optic atrophy)¹⁻³. The heterogeneous clinical presentations of mitochondrial carrier deficiencies may be explained by the wide range of different substrates transported by mitochondrial carriers and their different roles in intermediary metabolism¹.

SLC25A21 transports 2-oxoadipate and 2-oxoglutarate across the inner membrane of mitochondria by a counter-exchange mechanism⁶. We report a patient who presented with spinal muscular atrophy (SMA) and mitochondrial myopathy and we show that this is due to a dysfunctional mitochondrial oxodicarboxylate carrier (SLC25A21) caused by a homozygous c.695A>G mutation. Although the p.(Lys232Arg) amino acid change is conservative, we show that the novel pathogenic variant cannot transport substrates, demonstrating a direct functional link. We were able to identify the molecular aetiology of the disorder by combining computer-modelling of the effect of defective transport on central metabolism, targeted metabolomics and in vitro studies in human fibroblasts and neuronal cells.

MATERIALS AND METHODS

Whole exome sequencing

Exome sequencing was performed on blood DNA using the Illumina Truseq 62Mb exome capture kit and a HiSeq 2000. Duplicate sequence reads were removed with Fastuniq (v1.1) before alignment against the human UCSC hg38 reference genome using BWA (v0.7.12).

Coding bases had a mean read depth of 69.6-fold and 90.6% of these bases were covered to a minimum read depth of 10-fold. Sequence variants were called using Samtools/Bcftools (v1.3), followed by annotation with Annovar (Jan 2016 download) and filtering for rare, evolutionarily conserved, predicted damaging and with known mitochondrial function using custom Perl scripts and *in silico* effects were evaluated following the American College of Medical Genetics and Genomics guidelines⁷. The exome pipeline and variant filtering scripts are available from github (<https://github.com/Helgriff/Exome-Pipe>). Confirmation of the selected mutations was performed by Sanger sequencing.

SDS-PAGE and BN-PAGE analysis

For western blotting, whole cell lysates or mitochondrial extracts isolated from skeletal muscle tissue (50 µg) were separated by SDS-PAGE (12%). For BN-PAGE mitochondria were extracted from control and patient muscle as previously described⁸. The antibodies used are listed in **Supplementary file 1**).

Transport studies of SLC25A21 expressed in *Lactococcus lactis*

A codon-optimised *SLC25A21* gene was synthesized by GenScript (Piscataway, USA), and cloned into the expression vector pNZ8048 under the control of a nisin A-inducible promoter⁹. An N-terminal truncation of human oxodicarboxylate carrier ($\Delta 2-4$) was used to increase transport activity (**Supplementary file 1**. Supplementary methods and supplementary figure 2).

Transport assays were carried out using a Hamilton MicroLab Star robot (Hamilton Robotics Ltd). Transport of [¹⁴C]-2-oxoglutarate (American Radiolabeled Chemicals) was initiated by the addition of 100 µl PIPES buffer with 2.5 µM labeled 2-oxoglutarate (2.04 GBq/ mmol) to 5 µg fused membranes in a MultiScreenHTS-HA 96-well filter plate (pore

size 0.45 μm ; Millipore). The transport was stopped at 0, 60, 120, 300 sec, 10, 15, 20 and 30 min by the addition of 200 μl ice-cold PIPES buffer and filtering using a vacuum manifold, followed by two additional wash steps with 200 μl ice-cold PIPES buffer. Levels of radioactivity in the vesicles were measured by the addition of 200 μl MicroScint-20 (Perkin Elmer) and by quantifying the amount of radioactivity (TopCount scintillation counter, Perkin Elmer). Initial rates were determined using linear regression.

Computational modelling of SLC25A21 deficiency

Simulations of metabolism during impaired oxodicarboxylate transport were performed by using the MitoCore metabolic model¹⁰. Several alterations were made to the default model including the incorporation of five additional reactions involved in the production of tryptophan intermediates and the addition of seven ‘sinks’ to allow the efflux of tryptophan and lysine degradation intermediates: quinolinic acid, 2-oxoadipate, kynurenic acid, xanthurenic acid, L-2-aminoadipate, L-pipecolate and picolinic acid (the adapted model is available upon request). The default uptake parameters of two ‘fuel’ metabolites were altered to prevent their excessive uptake relative to oxygen availability; fatty acids (hexadecanoate) was set at a maximum uptake of 0.4 $\mu\text{mol}/\text{min}/\text{gDW}$ and the uptake of acetate was prevented. A minimum uptake flux of cytosolic L-lysine and L-tryptophan was set at a rate recorded experimentally for rat heart tissue¹¹. As two separate pathways exist to degrade lysine, the reaction for aminoadipate-semialdehyde synthase (ID:R_SACCD3m), part of the saccharopine pathway, was restricted to half of the uptake of lysine. To simulate SLC25A21 dysfunction, the representative transport steps in the model were disabled (IDs: R_2OXOADPTmB_MitoCore, R_2OXOADPTmC_MitoCore, R_2AMADPTmB_MitoCore, and R_2AMADPTmC_MitoCore). Further simulations were performed where the efflux of quinolinic acid and pipecolate were prevented. The system was simulated with Flux Balance

Analysis¹² using the objective function of maximum ATP production. Simulations were performed in MatLab (MathWorks, Inc., Natick, MA), using the COBRA toolbox¹² and the GLPK solver (<http://www.gnu.org/software/glpk/>).

Metabolite analysis by mass spectrometry

Metabolite measurements were performed by ultrahigh-performance liquid chromatography - tandem mass spectrometry (UPLC-MS/MS) on an Agilent 1290 UHPLC system coupled to a Sciex 4000 QTRAP mass spectrometer. For sample preparation, 45 µl of each sample was mixed with 105 µl of acetonitrile. After vortex mixing for 15 s and sonication in an ice-water bath for 1 min, the samples were centrifuged (14,000 x g, 10 min, 4 °C). The supernatants were used for quantitation of the metabolites using two different UPLC-MRM/MS methods, as described¹³ (**Supplementary file 1**, Supplementary methods).

Cell culture studies

Age-matched control and patient fibroblasts from the Newcastle Biobank were grown in high glucose Dulbecco's modified Eagle's medium (DMEM, Sigma, Poole, UK) supplemented with 10% FBS and 1% penicillin/streptomycin. SH-SY5Y cells were grown in Dulbecco's modified Eagle's medium (DMEM) supplemented with 10% fetal bovine serum, 2 mM glutamine, and 1% penicillin/streptomycin. Blue native polyacrylamide gel electrophoresis (BN-PAGE) of the mitochondrial respiratory chain complexes was performed as described previously¹⁴. For drug toxicity studies growth medium was supplemented with 5 and 50 µM 2-oxoadipic acid (Sigma 75447) and quinolinic acid (Sigma) respectively for 4 days before analysis. Experiments were done in triplicates.

Study of apoptosis in cell cultures with Annexin V-FITC/Propidium Iodide staining

Cell apoptosis was assessed using an Annexin V-FITC/Propidium Iodide (PI) Apoptosis Detection Kit (Abcam)(**Supplementary file 1**, Supplementary methods)

Quantification of mitochondrial DNA copy number

Quantification of mtDNA copy number was performed using CFX96 Touch™ Real-Time PCR Detection System (Bio-Rad) in triplicate by duplex TaqMan qPCR amplification of the mitochondrial gene *MTND1* and the nuclear encoded gene *B2M* as described previously¹⁵.

RESULTS

Patient

Written consent for the study and for photos was provided by the patient and family members, and approved by the local ethics committee (REC 13/YH/0310).

The patient is a 19-year-old daughter (**Fig. 1a**) of consanguineous Pakistani parents. She was born at full term with a weight of 3180 g, had normal early development and was walking by 15 months. Between age 3 and 5 years her walking deteriorated slowly with frequent falls. Aged 5 years her small hand muscles became wasted and clawed, and she developed bilateral foot drop, failure to thrive and scoliosis. On examination, mild facial weakness and tongue fasciculations were noted. Proximal muscle strength was normal, but distal muscle weakness and atrophy in both hands and feet were present. Deep tendon reflexes were brisk in the lower limbs with clonus at the ankles. She was walking with foot drop. Forced vital capacity (FVC) was 0.74L (56% of predicted normal value) in a sitting position.

Between 8-15 years of age, she deteriorated further with proximal weakness, intermittent relapses triggered by fever, and became wheelchair-bound at age 15. At age 18 she had developed severe weakness (2/5 MRC grade) resulting in inability to stand with absent deep tendon reflexes. Pulmonary function testing showed a FVC of 65%.

Routine laboratory tests were unremarkable, including renal and liver function, except for a constant microcytic anaemia (mean corpuscular volume: 53.9-55.9 fl; haemoglobin 8.6-10.5 g/dl; hematocrit 0.306-0.340%). She had normal levels of creatine kinase (CK), lactate, folate, vitamin E and B₁₂, very long chain fatty acids and phytanic acid. White cell enzymes were normal, including hexoseaminidase and arylsulfatase. Analyses of amino acids in serum and urine showed a slight, but reproducible increase in lysine, histidine, threonine, serine, glycine, tyrosine, cysteine dimer, alanine and asparagine. Analyses of the organic acids in urine showed some lactic aciduria and slightly increased excretion of 3-hydroxyisovaleric and glutaric acids. Plasma free and total carnitine levels were within acceptable ranges. Cerebrospinal fluid (CSF) was acellular with normal protein and amino acids, but lactate was marginally elevated (2.09 mmol/l versus normal of less than 2 mmol/l). Cranial and spinal MRIs were unremarkable.

Neurophysiological examination showed severe neurogenic change consistent with an anterior horn cell process. A nerve biopsy suggested an axonopathy, with mild and patchy loss of myelinated fibres. Electron microscopy showed many fibres accumulating membranous and granule debris, and glycogen deposits in the cytoplasm of the Schwann cells (data not shown).

Genetic analysis of the patient's exome

Exome sequencing of the patient's genomic DNA identified three homozygous rare missense variants in *SLC25A21*, *DTNA* and *HCCS* (minor allele frequency < 0.01) that were predicted as "probably damaging" by SIFT, Polyphen-2, LRT, Mutation Taster, FATHMM, PROVEAN and CADD. Segregation analysis in the patient, both parents and an unaffected sister showed segregation only with the c.695A>G; p.(Lys232Arg) mutation in *SLC25A21*, encoding the mitochondrial oxodicarboxylate carrier protein (*SLC25A21*)(**Fig. 1b**), which

transports 2-oxoadipate into the mitochondrion in exchange for oxoglutarate. This mutation was absent from the ExAC control database (<http://exac.broadinstitute.org/>), but reported in gnomAD as a heterozygous variant in a single individual from South Asia (<http://gnomad.broadinstitute.org/variant/14-37154039-T-C>). This region encompasses the patient's Pakistani heritage and suggests she may not be a unique case amongst this population. To identify further undiagnosed cases of mitochondrial oxodicarboxylate carrier deficiency, we searched for patients with a similar phenotype and carrying mutations in the *SLC25A21* gene in various international match-making databases, including RD-CONNECT (<http://rd-connect.eu/>), GeneMatcher (<http://genematcher.org>) and Matchmaker Exchange (www.matchmakerexchange.org), but we did not identify any other cases suggesting the rarity of this disease. The exome sequencing data were deposited in the RD-CONNECT database. We studied the effect of this mutation on the expression and function of the *SLC25A21* protein.

Skeletal muscle biopsy

A muscle biopsy at 8 years of age suggested neurogenic atrophy with grouping of smaller predominantly type I fibres and increased adipose tissue. (**Fig. 1c**) Oxidative enzyme histochemistry revealed numerous cytochrome *c* oxidase (COX) deficient fibres (**Fig. 1d**) with direct biochemical assay of respiratory chain function revealing decreased activities of complex I (0.026 nmols/ UCS, normal range 0.104 ± 0.036 nmols/ UCS) and complex IV (0.231×10^{-3} K.sec⁻¹.unit citrate synthase⁻¹, normal range 1.124 ± 0.511) with normal activities of complex II and III. A significant decrease in quantitative mtDNA levels (<10% of aged-matched controls) was detected in muscle by RT-PCR, suggesting mtDNA depletion (**Supplementary file 1**, Supplementary figure 3), although screening of the *TK2*, *RRM2B* and *POLG* genes encoding proteins involved in mtDNA maintenance failed to detect any

candidate pathogenic variants. Her karyotype was normal and deletion of *SMN1* was excluded.

Decreased steady-state levels of multiple respiratory chain complexes in skeletal muscle, but not in fibroblasts

Immunoblotting for mitochondrial proteins in skeletal muscle detected decreased steady-state levels of subunits of complexes I, IV and V, which was confirmed on blue-native polyacrylamide gel-electrophoresis (BN-PAGE) (**Fig. 2a-d**). The involvement of complexes I, IV and V but not complex II suggests a defect involving mtDNA expression or translation, since complex II is the only OXPHOS complex which does not contain subunits encoded by mtDNA. No significant decrease in the expression of the mitochondrial respiratory chain complexes was detected in fibroblasts. Reduced levels of SLC25A21 was found by immunoblotting in the patient's fibroblasts suggesting that the mutation slightly affects expression or turnover of the protein (**Fig. 2e-g**).

The p.(Lys232Arg) variant inactivates the transport function of SLC25A21

Mitochondrial carriers, like SLC25A21, have a single substrate binding site and a cytoplasmic and matrix salt bridge network, which regulate access to the substrate binding site from either side of the membrane¹⁶. The pathogenic p.(Lys232Arg) variant affects the matrix salt bridge network of the SLC25A21, as Lys232 is predicted to form a salt bridge interaction with Glu130 of the neighbouring domain (**Fig. 3a**). Although the predicted amino acid substitution is conservative, it may prevent the interaction or cause other interactions that may ablate the function of the protein (**Fig. 3b**). To study the effect of the genetic variant on transport of 2-oxoglutarate, truncated versions of the human wild-type and disease variant p.(Lys232Arg) were expressed in the cytoplasmic membrane of *Lactococcus lactis* under control of the Nisin

A promoter¹⁷. Expression levels of the wild-type and the p.(Lys232Arg) variant were similar, indicating the mutation does not affect expression and insertion of the carrier in *lactococcal* membranes (**Fig. 3d**). Wild-type SLC25A21 transported 2-oxoglutarate at a similar rate as the orthologous yeast ODC1 and ODC2 as measured by the uptake of [¹⁴C]-labelled 2-oxoglutarate into fused membrane vesicles in exchange for incorporated unlabelled substrate¹⁸. In contrast, the p.(Lys232Arg) variant of SLC25A21 did not transport 2-oxoglutarate above background levels, indicating that the function of the transport protein was completely impaired (**Fig. 3c**). This is consistent with the equivalent mutation in the bovine mitochondrial oxoglutarate carrier, p.(Lys244Arg), which also showed no discernible uptake above background¹⁸. The matrix salt bridge network is a highly conserved feature of mitochondrial carriers and is critical for their function. Thus, we conclude that the p.(Lys232Arg) variant causes SLC25A21 deficiency.

Computational modelling of mitochondrial oxodicarboxylate carrier (SLC25A21) deficiency predicts build-up of degradation intermediates

To investigate the consequences of impaired oxodicarboxylate transport by SLC25A21, we simulated its effects using the MitoCore computer model of central metabolism¹⁰. The model provides comprehensive coverage of central metabolism, including pathways for the degradation of lysine and tryptophan. SLC25A21 is modelled as four separate transport steps to reflect its characterized substrate specificity (2-oxoadipate for oxoglutarate, L-2-aminoadipate for oxoglutarate) and forward and reverse directions⁶. We altered the model to allow the production and efflux of various lysine and tryptophan intermediates by including additional reactions and ‘sinks’. First, the model was simulated to maximise ATP production using a mixture of ‘fuel’ metabolites such as glucose, lactate, fatty acids and a forced minimum uptake of L-lysine and L-tryptophan approximated from physiological

measurements taken from rat heart tissue. The mitochondrial oxodicarboxylate carrier deficiency was then simulated by disabling the corresponding transport steps in the model. These simulations showed that although ATP production and respiratory chain fluxes were maintained, there was an increased accumulation of L-pipecolic acid and quinolinic acid, which are intermediates of tryptophan and lysine degradation (**Fig. 4a**). However, accumulation of other intermediates, such as L-kynuerine, xanthurenate, picolinate, L-2-aminoadipate and 2-oxoadipate, was not observed. To identify alternative metabolites, the efflux of L-pipecolic acid and quinolinic acid were disabled in separate simulations. These simulations identified the efflux of 2-oxoadipate as a plausible alternative, as it had no impact on ATP production or central metabolism in general.

Metabolic analysis detects increased levels of oxoadipate, quinolinic acid and pipecolic acid

Mass spectrometry-based analysis of urine samples derived from the mitochondrial oxodicarboxylate carrier deficient patient compared to unrelated controls showed increased 2-oxoadipate, quinolinic and pipecolic acid levels in urine samples, as predicted by the metabolic modelling (**Fig. 4b**). For comparison, we also studied three additional patients with distal spinal muscular atrophy who carried a mutation in dehydrogenase E1 and transketolase domain containing 1 (*DHTKD1*). *DHTKD1* is upstream from *SLC25A21* in the tryptophan and lysine amino acid degradation pathways (**Fig. 4a**)¹⁹, and, when dysfunctional, may cause similar metabolic changes. The observed elevation of oxoadipate, quinolinic and pipecolic acid levels in all of the patients supports the hypothesis that increases in these metabolites may contribute to spinal motor neuron abnormalities (**Fig. 4b**).

Increased levels of oxoadipate and quinolinic acid selectively impair neurons

We supplemented control fibroblasts and neuronal cells (SH-SY5Y) with oxoadipate and quinolinic acid in concentrations, similar to the levels detected in the patients. There was no significant defect observed in fibroblasts, but a significant decrease of mitochondrial respiratory chain complexes was noted in neuronal cells on combined oxoadipate and quinolinic acid administration, suggesting a toxic effect of these metabolites for neurons (**Fig. 5a-d**). In the treated neuronal cells mtDNA copy numbers showed a slight, but significant (<0.05) reduction (**Supplementary file 1**, Supplementary figure 4). Visualization of apoptotic cells stained with annexin V-FITC using confocal microscopy after 4 days of treatment with 50 μ M quinolinic acid and 5 μ M 2-oxoadipate showed apoptosis in SHSY-5Y cells, while no apoptotic cells were detected in fibroblasts (**Fig. 5e**).

DISCUSSION

We report a patient with a novel mitochondrial disease affecting predominantly the spinal motor neurons and skeletal muscle due to dysfunction of the mitochondrial oxodicarboxylate carrier (SLC25A21). Interestingly, a 14q13.3 deletion involving the *SLC25A21* gene has been reported with familial synpolydactyly²⁰. However, this was suggested to occur due to the deletion of regulatory elements of the neighbouring developmental genes *PAX9* and *MIPOLI*, which occur within introns of the *SLC25A21* gene. Our patient did not have synpolydactyly, probably because the *PAX9* and *MIPOLI* regulatory elements are unaffected. The patient presented with a wide range of metabolic and tissue specific mitochondrial abnormalities, including mitochondrial respiratory chain deficiencies involving complexes I and IV, associated mtDNA depletion and metabolic abnormalities. Pathogenic variants in another mitochondrial carrier *SLC25A4* affecting most likely the substrate binding and mechanics of the carrier also present with severe mtDNA depletion which was explained by a deficiency of

ADP/ATP transport²¹. However, in contrast to mutations in *SLC25A4*, the oxodicarboxylate carrier is not directly involved in mitochondrial nucleotide transport.

The disease is caused by the homozygous p.(Lys232Arg) mutation, which affects the highly conserved matrix salt bridge network motif PX[DE]XX[RK] and impairs oxodicarboxylate transport¹⁸. An equivalent mutation in the mitochondrial oxoglutarate carrier (p.Lys244Arg) also leads to a dysfunctional protein¹⁸. Mitochondrial carriers cycle between a matrix and cytoplasmic state, and the matrix network closes the carrier to the mitochondrial matrix, when the carrier is in the cytoplasmic state²². Although the arginine substitution will conserve the positive charge, it could impair network formation by changing the salt bridge geometry or by introducing additional polar interactions. We propose that the mutation causes mitochondrial oxodicarboxylate carrier deficiency since transport is completely abolished, leading to several metabolic abnormalities, which are causative for the severe, tissue specific defect of mitochondrial respiratory chain enzymes and result in tissue specific mtDNA depletion. However, we cannot exclude the possibility that the variant was not the sole cause of the phenotype²³.

To investigate the consequences of mitochondrial oxodicarboxylate carrier deficiency on metabolism, we simulated its effects using the MitoCore computer model of central metabolism¹⁰. The simulations predicted that three metabolites would accumulate: 2-oxoadipate, L-pipecolic and quinolinic acid. Targeted metabolic analysis by mass spectroscopy confirmed the modelling results by showing an increase in the levels of these metabolites in the patient's urine. To corroborate a pathogenic role for these amino acid degradation intermediates in spinal motor neurons, we performed metabolic testing in three previously reported¹⁹ patients who carried a pathogenic variant in the gene for dehydrogenase E1 and transketolase domain containing 1 (*DHTKD1*) gene an enzyme that is part of both lysine and tryptophan degradation pathways, and catalyses the decarboxylation of 2-

oxoadipate to glutaryl-CoA. Mutations in *DHTKD1* can be asymptomatic or cause 2-aminoadipic 2-oxoadipic aciduria (AMOXAD), resulting in symptoms including a mild to severe neurological phenotypes, such as muscular hypotonia, or autosomal dominant peripheral neuropathy^{24,25} and decreased mtDNA copy number, which could be due to reduced mitochondrial biogenesis²⁶. However, *DHTKD1* dysfunction as a cause of inherited peripheral neuropathy is still debated due to these heterogeneous clinical presentations. Our results show, that the levels of all three metabolites were elevated, which is consistent with literature reports of patients with *DHTKD1* deficiency²⁴. The lower levels of 2-oxoadipate seen in the urine of these patients compared to *SLC25A21* deficiency is presumably due to the transport of 2-oxoadipate into the mitochondrial matrix where it cannot be excreted.

Pipecolic acid levels are increased in several related peroxisome disorders including Zellweger Syndrome²⁷, infantile Refsum disease²⁸ and neonatal adrenoleukodystrophy²⁹, as well as the lysine degradation disorder hyperlysinemia type I³⁰, caused α -aminoadipate semialdehyde synthase deficiency. Zellweger Syndrome presents with neurological dysfunction, craniofacial abnormalities, and liver dysfunction³¹, infantile Refsum disease presents with retinitis pigmentosa, peripheral neuropathy, cerebellar ataxia²⁸, neonatal adrenoleukodystrophy presents with hypotonia and convulsions²⁹, whereas hyperlysinemia presents with seizures and mildly delayed psychomotor development³⁰. Despite these disorders sharing a common phenotype of neurological dysfunction, it has been suggested that in Zellweger Syndrome raised pipecolic acid levels are not the direct cause of pathology but arise as a benign consequence³¹ and cases of hyperlysinemia type I have been reported to be asymptomatic³².

Quinolinic acid is a precursor for NAD⁺ biosynthesis³³⁻³⁵, and so may have contributed to some of the patient's mitochondrial abnormalities due to a NAD⁺ deficiency. It is also a potent neurotoxin with high tendency to form free radicals, and is involved in several

neuroinflammatory disorders^{36,37}. Quinolinic acid at elevated concentrations causes DNA damage, NAD⁺ depletion, increased nitric oxide formation, and cell death in neurons and astrocytes³³. Quinolinic acid exerts its cytotoxicity³⁷ by causing over-stimulation of the *N*-methyl-D-aspartate (NMDA) receptor, which through free radicals leads to irreversible inhibition of complex I, complex II, ATP synthase, aconitase, creatine kinase, superoxide dismutase and mitochondrial DNA damage³⁸. In addition, quinolinic acid forms a complex with Fe²⁺³²⁻³⁴ that may result in iron sequestration and probably resulted in the microcytic anaemia in the SLC25A21-deficient patient. Quinolinic acid also depletes glutathione in astrocytes via peroxynitrite, causing significant decreases in activity of complexes I and II³⁹, which is consistent with the biochemical tests on our patient's respiratory complexes. The presence of elevated lactate levels in the cerebrospinal fluid of the patient may be related to the mitochondrial enzyme defect, but may also be consistent with the increased lactate dehydrogenase (LDH) activity seen with quinolinic acid neurotoxicity^{33,34,36-39}.

Lastly, we tested the effect of quinolinic acid and 2-oxoadipate on neuronal cells and fibroblasts. There was a significant decrease of mitochondrial respiratory chain complexes in neuronal cells, but not fibroblasts, whereas apoptotic cells were only seen with a combination of the two metabolites in neuronal cells. We also detected a significant decrease in mtDNA copy number in the treated neurons (Supplementary file 1, Supplementary figure 4). In HepG2 cells with DHTKD1 silenced, a decrease in mtDNA copy number was reported and ascribed to reduced mitochondrial biogenesis²⁶. Given that DHTKD1 and SLC25A21 are part of the same pathway, they may share common disease mechanisms, e.g. due to quinolate accumulation. Another example of a metabolic defect in the TCA cycle associated with low mtDNA copy numbers are mutations in *SUCLA2* resulting in mitochondrial encephalomyopathy and mtDNA depletion.

Our data suggest that 2-oxoadipate and quinolinic acid are selectively toxic for spinal motor neurons and their increased levels through disrupted tryptophan and lysine degradation may contribute to neuropathy.

In light of our findings, we have initiated a low lysine and tryptophan diet for the patient, which is used to treat glutaric aciduria type I⁴⁰ although so far without significant clinical benefit in the patient. Follow-up examinations of the patient will enable a better estimation of the efficacy of dietary interventions.

In summary, we combined a wide range of genetic, biochemical, molecular, metabolic and bioinformatics techniques to pinpoint the pathomechanism resulting from a novel mitochondrial carrier protein deficiency. Each of these techniques were needed to support the molecular diagnosis, highlighted important targets and helped to better understand the pathomechanism of disease in this patient, and also provided important insights for studies in other neurological and metabolic diseases.

AUTHOR CONTRIBUTIONS

VB, MSK, ACS, FE and AJR performed the experiments, analysed the data and participated in the drafting of the manuscript, BB, VR and RGW provided clinical information, AR and CB performed for the metabolic testing, ML, AP and HG did the bioinformatics evaluation and segregation analysis, TP, MO and RWT provided data on the muscle biopsy, HL and PFC participated in drafting and revision of the manuscript, ERSK and RH participated in the study design, data analysis and drafted and revised the manuscript.

ACKNOWLEDGEMENTS

RH is a Wellcome Trust Investigator (109915/Z/15/Z), who receives support from the the Wellcome Centre for Mitochondrial Research (203105/Z/16/Z), Medical Research Council (UK) (MR/N025431/1), the European Research Council (309548), the Wellcome Trust Pathfinder Scheme (201064/Z/16/Z), the Newton Fund (UK/Turkey, MR/N027302/1). HL receives funding from the European Union Seventh Framework Programme (FP7/2007–2013) under grant agreement No. 305444 (RD-Connect) and 305121 (Neuromics). AR acknowledges the financial support by the Ministerium für Innovation, Wissenschaft und Forschung des Landes Nordrhein-Westfalen, the Senatsverwaltung für Wirtschaft, Technologie und Forschung des Landes Berlin, and the Bundesministerium für Bildung und Forschung. RWT is supported by the Wellcome Centre for Mitochondrial Research (203105/Z/16/Z), the Medical Research Council (MRC) Centre for Translational Research in Neuromuscular Disease, Mitochondrial Disease Patient Cohort (UK) (G0800674), the Lily Foundation and the UK NHS Highly Specialised Service for Rare Mitochondrial Disorders of Adults and Children. This research was funded by the Medical Research Council through programme grant MC_U105663139 to MSK and ERSK and MC_U105674181 to ACS, FE

and AJR. RH and ERSK also gratefully acknowledge the Marie-Curie Initial Training Networks (ITN) grant 'MEET' (Mitochondrial European Educational Training Project, Grant Agreement no. 317433) for the collaboration.

LEGENDS FOR FIGURES

Figure 1. Clinical and laboratory investigations in the patient

(a) The patient has a severe distal and proximal weakness affecting the hands and feet and she is wheelchair bound. (b) Sanger sequencing detected the homozygous c.695A>G, p.(Lys232Arg) mutation in the patient, while both parents were heterozygous carriers of this mutation, and the healthy sister was wild type. (c) Muscle histology showed some groups of atrophic fibres and groups of hypertrophic fibres, typically seen in spinal muscular atrophy. ATPase pH 4.2 staining demonstrates a significant type grouping, in support of the neurogenic atrophy. (d) H&E, COX, SDH, COX-SDH; COX is generally weak across the section, also detected in the sequential assay.

Figure 2. Immunoblotting and BN-PAGE in skeletal muscle and fibroblasts

(a-b) In skeletal muscle immunoblotting detected decreased steady-state levels of mitochondrial OXPHOS complex subunits for complexes I, III, IV and V. (c-d) BN-PAGE detected reduced complexes I, IV and V. (e) Immunoblotting detected slightly reduced SLC25A21 in the patient's fibroblasts, while (f) mitochondrial OXPHOS proteins were normal. (g) BN-PAGE detected normal respiratory chain complexes in the patient's cell line. Nuclear-encoded GAPDH, VDAC, SDHA or SDHB proteins were used as loading controls. Abbreviations: Complex I (CI); complex II (CII); complex III (CIII); complex IV (CIV); complex V / F₁F₀ ATP synthase (CV); (GAPDH); cytochrome *c* oxidase 1 (COX1); cytochrome *c* oxidase 2 (COX2); voltage-dependent anion-selective channel (VDAC); NADH dehydrogenase ubiquinone 1 beta subcomplex subunit 8 (NDUFB8); F₁F₀ ATP synthase subunit (ATP5A); succinate dehydrogenase subunit A (SDHA); succinate dehydrogenase subunit B (SDHB); ubiquinol-cytochrome *c* reductase core protein II (UQCRC2).

Figure 3. The p.(Lys232Arg) mutation interferes with the formation of the matrix salt bridge network and impairs function of the mitochondrial oxodicarboxylate carrier (SLC25A21).

(a) Membrane view of the comparative homology model of human SLC25A21 generated with SwissModel (Arnold et al., 2006) based on the structure of the bovine ADP/ATP carrier (alignment shown in **Supplementary file 1**. Supplementary figure 1). The matrix and cytoplasmic salt bridge network are shown in dark blue and cyan, respectively. The mutated lysine 232 is shown in yellow. The residues of the proposed substrate binding site are shown in green and the substrate 2-oxoglutarate is shown in an orange ball and stick representation.

(b) Cytoplasmic view showing the residues involved in the formation of the matrix salt bridge network in dark blue. The most probable side chain conformations of the p.(Lys232Arg) mutation are shown in magenta, indicating that the substitution might impair binding to Glu131 and might lead to other polar interactions.

(c) The 2-oxoglutarate uptake curves of SLC25A21 and SLC25A21_p.(Lys232Arg). Fused membrane vesicles of *Lactococcus lactis* expressing SLC25A21 (triangles) or SLC25A21_p.(Lys232Arg) (circles) were pre-loaded with 5 mM 2-oxoglutarate and transport was initiated with the external addition of 1.5 μ M [14 C]-2-oxoglutarate. Membranes of the uninduced SLC25A21 strain (squares) show background binding, indicating that SLC25A21_p.(Lys232Arg) does not transport above background.

(d) Expression levels of the wild-type and mutant SLC25A21 were similar, indicating the mutation did not affect expression and insertion of the carrier in lactococcal membranes.

(e) The 2-oxoglutarate transport rates of SLC25A21 and SLC25A21_p.(Lys232Arg) after correction for background binding. The error bars represent the standard deviation of four technical repeats. Student t-tests, significant uptake above background: $P > 0.05$, not significant (NS); $P > 0.01$, *; $P > 0.001$, **; $P > 0.0001$, ***; $P < 0.0001$, ****.

Figure 4. Metabolism of tryptophan and lysine is impaired by mitochondrial oxodicarboxylate carrier deficiency.

(a) The degradation pathways of tryptophan and lysine runs through the mitochondrion, which links it to the generation of ATP through the production of NADH, which leads to the reduction of the co-enzyme Q (Q) via complex I, the production of acetyl-CoA, which enters the TCA cycle, and through the reduction of the Q pool directly via glutaryl-CoA dehydrogenase and the electron-transferring flavoprotein (dashed line). The metabolic model predicts an increase in quinolinic acid and picolinate levels, which are spontaneously (*) formed from semi-aldehydes, and in oxoadipate and pipecolate levels, as the import of 2-oxoadipate and 2-aminoadipate into mitochondria is blocked by mitochondrial oxodicarboxylate carrier deficiency (red arrows). These intermediates may have neurotoxic effects, leading to neuropathy. (b) Targeted metabolic analysis detected increased 2-oxoadipate, quinolinic acid and pipecolic acid in the patient and in three other patients carrying *DHTKDI* mutations.

Figure 5. Administration of 2-oxoadipate and quinolinic acid *in vitro* was more toxic for neuronal cells than fibroblasts

(a) Western blot analysis detected normal expression in control fibroblasts after supplementation of 50 μ M quinolinic acid and 5 μ M 2-oxoadipate after 4 days. (b) Quantification of protein levels were normalised to porin. (c) In human neuroblastoma cells (SHSY-5Y) the supplementation of the 50 μ M quinolinic acid and 5 μ M 2-oxoadipate resulted in significantly reduced levels affecting all five OXPHOS complexes, as shown in (d) (n=3 experimental replicates). P values are from One-Way ANOVA test. Where indicated * P<0.05. (e) Visualization of apoptotic cells stained with annexin V-FITC using confocal

microscopy after treatment with only 50 μ M quinolinic acid and combination of 50 μ M quinolinic acid and 5 μ M 2-oxoadipate. Cells were supplemented for 4 days before staining. DAPI staining was used as nuclear marker. Top row shows fibroblasts where no Annexin V positive cells were detected in any treatment. Bottom row shows SHSY-5Y cells: Indication annexin V positive cells were identified after double supplementation. Scale bar = 50 μ M.

Supplementary file 1 contains Supplementary methods and 4 Supplementary figures.

References

- 1 Palmieri, F. Mitochondrial transporters of the SLC25 family and associated diseases: a review. *J Inherit Metab Dis* **37**, 565-575, doi:10.1007/s10545-014-9708-5 (2014).
- 2 Shamseldin, H. E. *et al.* Mutation of the mitochondrial carrier SLC25A42 causes a novel form of mitochondrial myopathy in humans. *Hum Genet* **135**, 21-30, doi:10.1007/s00439-015-1608-8 (2016).
- 3 Abrams, A. J. *et al.* Mutations in SLC25A46, encoding a UGO1-like protein, cause an optic atrophy spectrum disorder. *Nat Genet* **47**, 926-932, doi:10.1038/ng.3354 (2015).
- 4 Wibom, R. *et al.* AGC1 deficiency associated with global cerebral hypomyelination. *N Engl J Med* **361**, 489-495, doi:10.1056/NEJMoa0900591 (2009).
- 5 Mayr, J. A. *et al.* Deficiency of the mitochondrial phosphate carrier presenting as myopathy and cardiomyopathy in a family with three affected children. *Neuromuscul Disord* **21**, 803-808, doi:10.1016/j.nmd.2011.06.005 (2011).
- 6 Fiermonte, G. *et al.* Identification of the human mitochondrial oxodicarboxylate carrier. Bacterial expression, reconstitution, functional characterization, tissue distribution, and chromosomal location. *J Biol Chem* **276**, 8225-8230, doi:10.1074/jbc.M009607200 (2001).
- 7 Rehm, H. L. *et al.* ACMG clinical laboratory standards for next-generation sequencing. *Genet Med* **15**, 733-747, doi:10.1038/gim.2013.92 (2013).
- 8 Olahova, M. *et al.* LRPPRC mutations cause early-onset multisystem mitochondrial disease outside of the French-Canadian population. *Brain* **138**, 3503-3519, doi:10.1093/brain/awv291 (2015).
- 9 King, M. S., Boes, C. & Kunji, E. R. Membrane protein expression in *Lactococcus lactis*. *Methods in enzymology* **556**, 77-97, doi:10.1016/bs.mie.2014.12.009 (2015).

- 10 Smith, A. C., Eyassu, F., Mazat, J.-P. & Robinson, A. J. MitoCore: A curated constraint-based model for simulating human central metabolism. *BioRxiv* doi:10.1101/141101 (2017).
- 11 Banos, G., Daniel, P. M., Moorhouse, S. R., Pratt, O. E. & Wilson, P. A. The influx of amino acids into the heart of the rat. *J Physiol* **280**, 471-486 (1978).
- 12 Becker, S. A. *et al.* Quantitative prediction of cellular metabolism with constraint-based models: the COBRA Toolbox. *Nat Protoc* **2**, 727-738, doi:10.1038/nprot.2007.99 (2007).
- 13 Han, J., Gagnon, S., Eckle, T. & Borchers, C. H. Metabolomic analysis of key central carbon metabolism carboxylic acids as their 3-nitrophenylhydrazones by UPLC/ESI-MS. *Electrophoresis* **34**, 2891-2900, doi:10.1002/elps.201200601 (2013).
- 14 Bartsakoulia, M. *et al.* Cysteine supplementation may be beneficial in a subgroup of mitochondrial translation deficiencies. *J Neuromuscul Dis* **3**, 363-379, doi:10.3233/JND-160178 (2016).
- 15 Blakely, E. *et al.* Novel mutations in the TK2 gene associated with fatal mitochondrial DNA depletion myopathy. *Neuromuscul Disord* **18**, 557-560, doi:10.1016/j.nmd.2008.04.014 (2008).
- 16 King, M. S., Kerr, M., Crichton, P. G., Springett, R. & Kunji, E. R. Formation of a cytoplasmic salt bridge network in the matrix state is a fundamental step in the transport mechanism of the mitochondrial ADP/ATP carrier. *Biochimica et biophysica acta* **1857**, 14-22, doi:10.1016/j.bbabi.2015.09.013 (2016).
- 17 Monne, M., Chan, K. W., Slotboom, D. J. & Kunji, E. R. Functional expression of eukaryotic membrane proteins in *Lactococcus lactis*. *Protein Sci* **14**, 3048-3056, doi:10.1110/ps.051689905 (2005).

- 18 Cappello, A. R. *et al.* Functional and structural role of amino acid residues in the odd-numbered transmembrane alpha-helices of the bovine mitochondrial oxoglutarate carrier. *J Mol Biol* **369**, 400-412, doi:10.1016/j.jmb.2007.03.048 (2007).
- 19 Bansagi, B. *et al.* Genetic heterogeneity of motor neuropathies. *Neurology* **88**, 1226-1234, doi:10.1212/WNL.0000000000003772 (2017).
- 20 Meyertholen, K., Ravnan, J. B. & Matalon, R. Identification of a novel 14q13.3 deletion involving the SLC25A21 gene associated with familial synpolydactyly. *Mol Syndromol* **3**, 25-29, doi:10.1159/000339177 (2012).
- 21 Thompson, K. *et al.* Recurrent de novo dominant mutations in SLC25A4 cause severe early-onset mitochondrial disease and loss of mitochondrial DNA copy number. *Am J Hum Genet* **99**, 860-876, doi:10.1016/j.ajhg.2016.08.014 (2016).
- 22 Pebay-Peyroula, E. *et al.* Structure of mitochondrial ADP/ATP carrier in complex with carboxyatractyloside. *Nature* **426**, 39-44, doi:10.1038/nature02056 (2003).
- 23 MacArthur, D. G. *et al.* Guidelines for investigating causality of sequence variants in human disease. *Nature* **508**, 469-476, doi:10.1038/nature13127 (2014).
- 24 Danhauser, K. *et al.* DHTKD1 mutations cause 2-amino adipic and 2-oxoadipic aciduria. *Am J Hum Genet* **91**, 1082-1087, doi:10.1016/j.ajhg.2012.10.006 (2012).
- 25 Xu, W. Y. *et al.* A nonsense mutation in DHTKD1 causes Charcot-Marie-Tooth disease type 2 in a large Chinese pedigree. *Am J Hum Genet* **91**, 1088-1094, doi:10.1016/j.ajhg.2012.09.018 (2012).
- 26 Xu, W. *et al.* DHTKD1 is essential for mitochondrial biogenesis and function maintenance. *FEBS letters* **587**, 3587-3592, doi:10.1016/j.febslet.2013.08.047 (2013).
- 27 Govaerts, L., Monnens, L., Tegelaers, W., Trijbels, F. & van Raay-Selten, A. Cerebro-hepato-renal syndrome of Zellweger: clinical symptoms and relevant laboratory findings in 16 patients. *Eur J Pediatr* **139**, 125-128 (1982).

- 28 Tranchant, C. *et al.* A new peroxisomal disease with impaired phytanic and pipecolic acid oxidation. *Neurology* **43**, 2044-2048 (1993).
- 29 Kelley, R. I. & Moser, H. W. Hyperpipecolic acidemia in neonatal adrenoleukodystrophy. *Am J Med Genet* **19**, 791-795, doi:10.1002/ajmg.1320190420 (1984).
- 30 Tondo, M. *et al.* Clinical, biochemical, molecular and therapeutic aspects of 2 new cases of 2-aminoadipic semialdehyde synthase deficiency. *Mol Genet Metab* **110**, 231-236, doi:10.1016/j.ymgme.2013.06.021 (2013).
- 31 Dancis, J. & Hutzler, J. The significance of hyperpipecolatemia in Zellweger syndrome. *Am J Hum Genet* **38**, 707-711 (1986).
- 32 Houten, S. M. *et al.* Genetic basis of hyperlysinemia. *Orphanet J Rare Dis* **8**, 57, doi:10.1186/1750-1172-8-57 (2013).
- 33 Braidy, N., Grant, R., Adams, S., Brew, B. J. & Guillemin, G. J. Mechanism for quinolinic acid cytotoxicity in human astrocytes and neurons. *Neurotox Res* **16**, 77-86, doi:10.1007/s12640-009-9051-z (2009).
- 34 Chen, Y., Brew, B. J. & Guillemin, G. J. Characterization of the kynurenine pathway in NSC-34 cell line: implications for amyotrophic lateral sclerosis. *J Neurochem* **118**, 816-825, doi:10.1111/j.1471-4159.2010.07159.x (2011).
- 35 Lugo-Huitron, R. *et al.* Quinolinic acid: an endogenous neurotoxin with multiple targets. *Oxid Med Cell Longev* **2013**, 104024, doi:10.1155/2013/104024 (2013).
- 36 Vamos, E., Pardutz, A., Klivenyi, P., Toldi, J. & Vecsei, L. The role of kynurenines in disorders of the central nervous system: possibilities for neuroprotection. *J Neurol Sci* **283**, 21-27, doi:10.1016/j.jns.2009.02.326 (2009).
- 37 Schwarcz, R. The kynurenine pathway of tryptophan degradation as a drug target. *Curr Opin Pharmacol* **4**, 12-17, doi:10.1016/j.coph.2003.10.006 (2004).

- 38 Brown, G. C. Regulation of mitochondrial respiration by nitric oxide inhibition of cytochrome c oxidase. *Biochimica et biophysica acta* **1504**, 46-57 (2001).
- 39 Barker, J. E., Bolanos, J. P., Land, J. M., Clark, J. B. & Heales, S. J. Glutathione protects astrocytes from peroxynitrite-mediated mitochondrial damage: implications for neuronal/astrocytic trafficking and neurodegeneration. *Dev Neurosci* **18**, 391-396 (1996).
- 40 Boy, N. *et al.* Low lysine diet in glutaric aciduria type I--effect on anthropometric and biochemical follow-up parameters. *J Inherit Metab Dis* **36**, 525-533, doi:10.1007/s10545-012-9517-7 (2013).

Conflict of Interest Statement

Mitochondrial oxodicarboxylate carrier deficiency is associated with mitochondrial DNA depletion and spinal muscular atrophy-like disease

Veronika Boczonadi PhD^{1*}, Martin S. King PhD^{2*}, Anthony C. Smith PhD², Monika Olahova PhD³, Boglarka Bansagi MD¹, Andreas Roos PhD^{1,4}, Filmon Eyassu PhD², Christoph Borchers PhD⁵, Venkateswaran Ramesh MD⁶, Hanns Lochmüller MD¹, Tuomo Polvikoski MD⁷, Roger G. Whittaker MD⁸, Angela Pyle PhD¹, Helen Griffin PhD¹, Robert W. Taylor PhD³, Patrick F. Chinnery FRCP, FMedSci^{2,9}, Alan J. Robinson PhD², Edmund R.S. Kunji PhD^{2*}, Rita Horvath MD, PhD^{1*}

The authors have no conflict of interest.



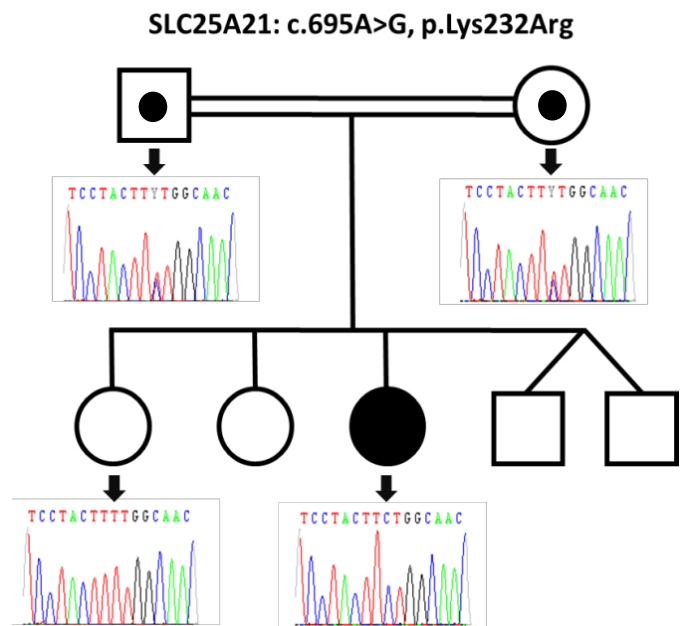
25/10/2017

Figure 1

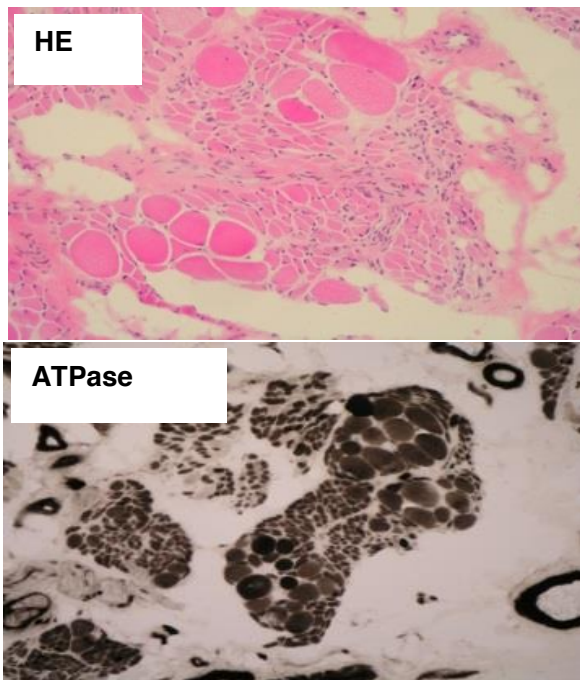
a



b



c



d

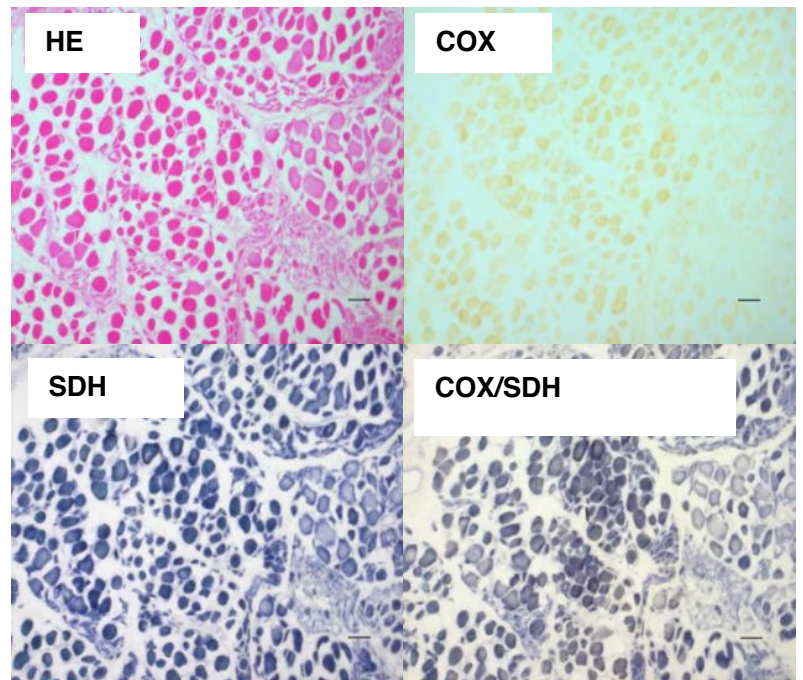


Figure 2

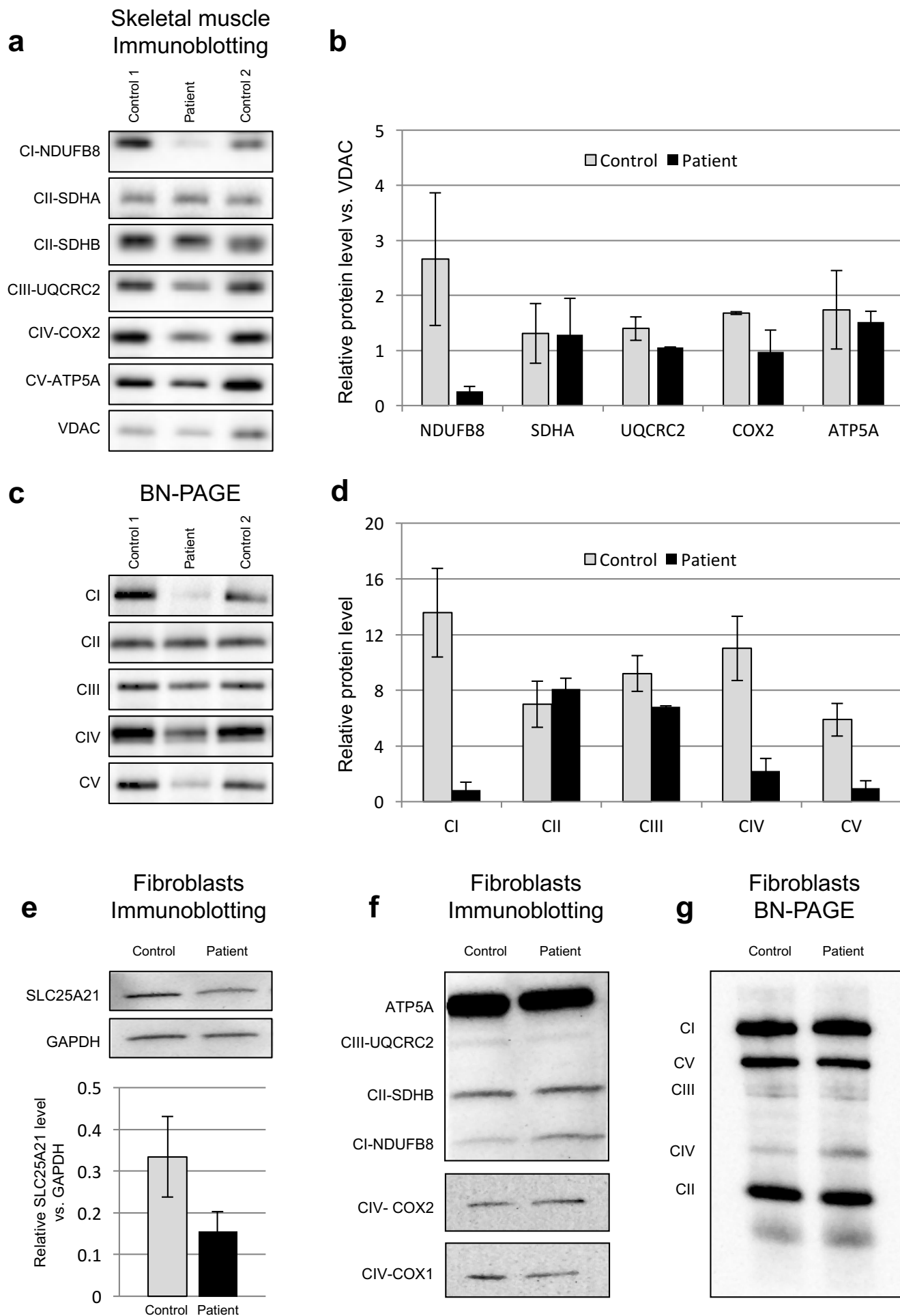


Figure 3

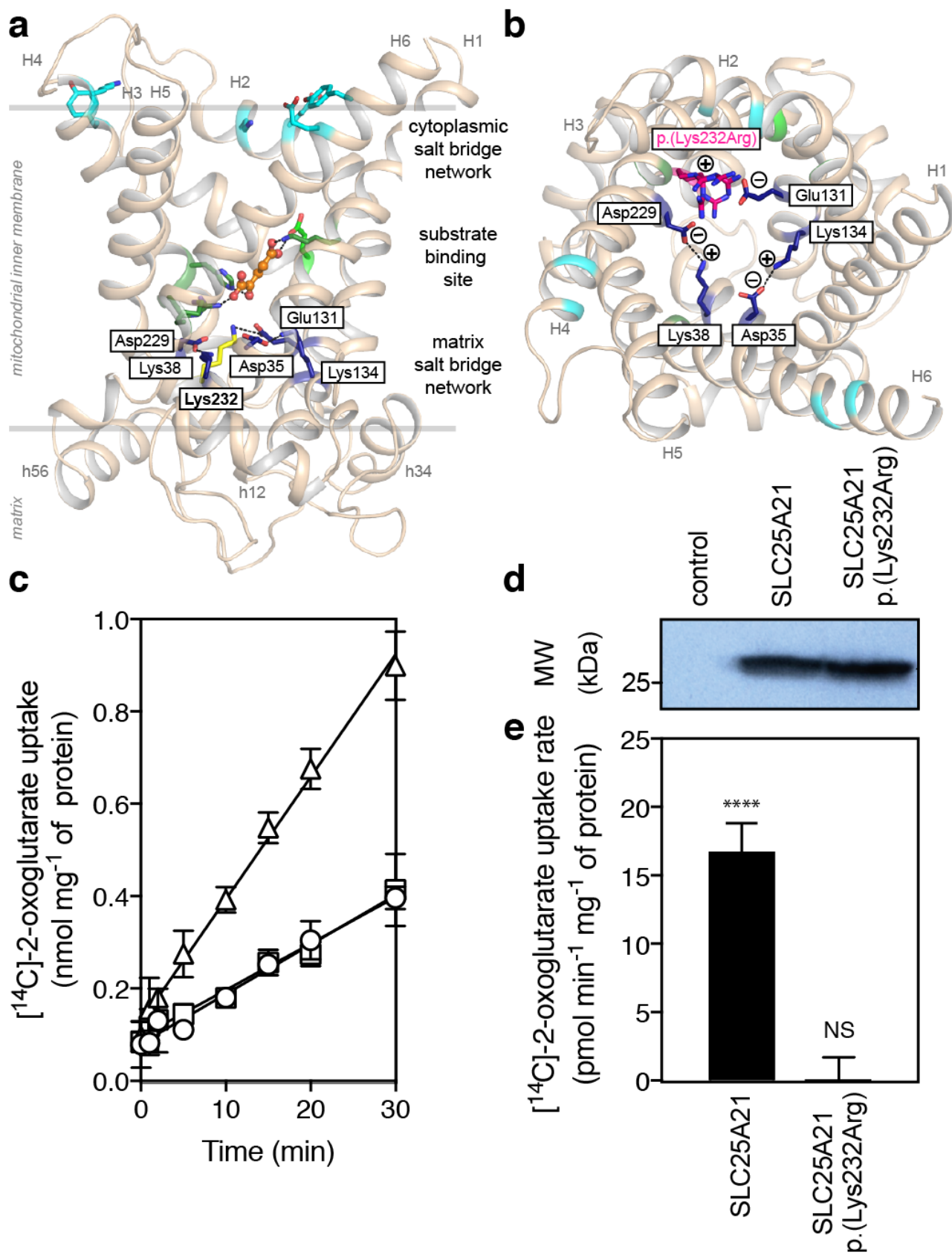
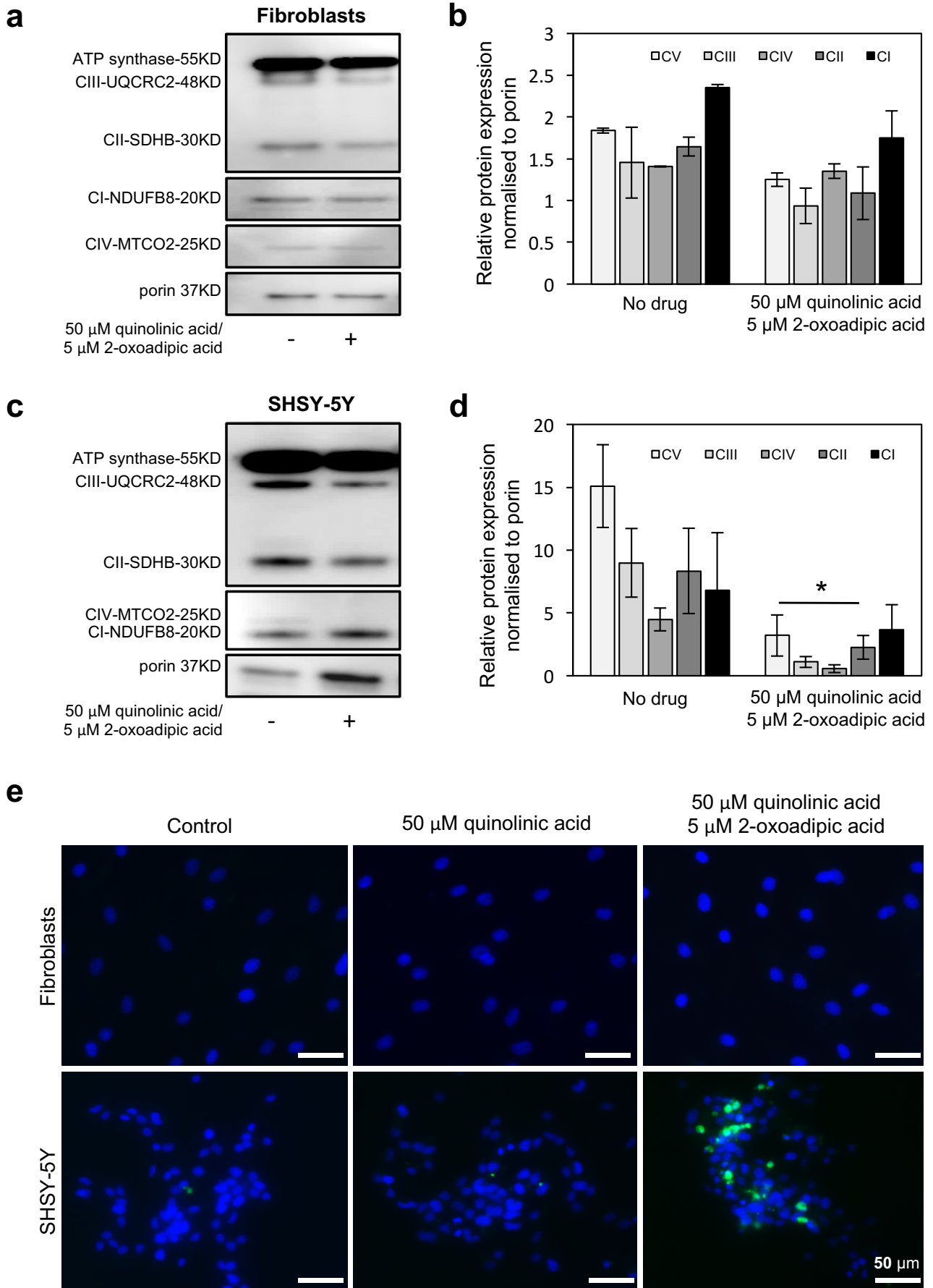


Figure 5



Supplementary information

Supplementary methods

SDS-PAGE and BN-PAGE analysis

100 µg of n-dodecyl-β-d-maltoside solubilised mitochondria were separated on 4-16% native polyacrylamide BisTris gel (Life Technologies) followed by an electrophoretic transfer and immunoblotting. OXPHOS subunits and complexes were detected using antibodies against NDUFB8 (ab110242, Abcam), SDHA (ab14715, Abcam), UQCRC2 (ab14745, Abcam), COX1 (ab14705, Abcam), ATP5A (ab14748, Abcam), OXPHOS cocktail (MS601 MitoSciences) and anti-mouse-HRP conjugated secondary antibodies (P0260, DAKO). VDAC (ab14734, Abcam) and GAPDH (Santa-Cruz sc-25778 HRP) were used as loading controls. An anti-SLC25A21 antibody produced in rabbit (ab167033, Abcam) was used at 1:1,000 dilution for one hour, followed by an anti-rabbit-HRP conjugate produced in goat (Millipore, AP132P) at 1:10,000 dilution for a further hour. The membranes were developed using Amersham ECL Western blotting detection system.

Transport studies of SLC25A21 expressed in *L. lactis*

The plasmid was transformed in *L. lactis* strain NZ9000 by electroporation. Vectors were isolated by miniprep (Qiagen), according to the manufacturer's instructions with one alteration; 10 mg/ml lysozyme was added to the lysis buffer and the resuspended cells were incubated at 55 °C for twenty minutes prior to lysis; successful transformants were confirmed by sequencing.

Pre-cultures of *L. lactis* were obtained by inoculating M17 medium supplemented with 1% (w/v) glucose and 5 µg/ml chloramphenicol from glycerol stocks and incubating the cultures overnight at 30 °C with no aeration. Cells were diluted to a starting A600 of 0.1 in fresh M17 medium supplemented with 1% (w/v) glucose and 5 µg/ml chloramphenicol and

incubated at 30 °C with no aeration until the A600 reached 0.5. Expression of the recombinant protein was induced by addition of nisin A with a dilution of 1:10,000 of spent M17 medium from nisin A-excreting *L. lactis* strain NZ9700. Cells were grown for a further 3 h at 30 °C, harvested by centrifugation (6000 x g, 10 min, 4 °C), resuspended in PIPES buffer (10 mM PIPES pH 7.0, 50 mM NaCl) and collected by centrifugation as before. Cells were subsequently resuspended in 50 ml PIPES buffer and disrupted mechanically with a cell disruptor (Constant Cell Disruption Systems) at 33 kpsi. Cell debris was removed by centrifugation (10,800 x g, 15 min, 4 °C), and the membranes collected by ultracentrifugation (138,000g, 1 h, 4 °C). Pellets were resuspended in PIPES buffer and stored in liquid nitrogen.

E. coli polar lipid extract and egg yolk phosphatidylcholine (20 mg/ml in chloroform) were mixed in a 3:1 mass ratio. The chloroform was evaporated under a stream of nitrogen, the lipids were resuspended in PIPES buffer with a homogenizer to a final concentration of 20 mg/ml and frozen in liquid nitrogen.

To make membrane fusions, 1 mg *L. lactis* membranes was mixed with 5 mg liposomes, diluted to a final volume of 900 µL with PIPES, and fused by seven cycles of freezing in liquid nitrogen and thawing at room temperature before storage in liquid nitrogen. The membrane vesicle fusions were thawed and 100 µl 50 mM 2-oxoglutarate added. Vesicles were extruded 11 times through a 1-µm polycarbonate filter, passed through a pre-equilibrated PD10 column to remove external substrate, collected in 1.6 ml PIPES buffer, and diluted four-fold before use.

Metabolite analysis by mass spectrometry

Quantitation of oxoadipate, quinolinic acid, glycolate, lactate, pyruvate, citrate, isocitrate, succinate, fumarate, malate, α -hydroxyglutarate and 2-oxoglutarate was carried out by pre-analytical chemical derivatization - UPLC-MRM/MS using 3-nitrophenylhydrazine (3-NPH)

as the derivatizing reagent as described. Quantitation of pipercolate and amino acids was performed by pre-analytical chemical derivatization – UPLC-MRM/MS using dansyl chloride as the derivatizing reagent. A stock solution that contained the standard substances of pipercolate and 21 amino acids, at an equal concentration of 1 mM, was prepared in 70% acetonitrile. This solution was diluted with the same solvent, and step by step at a same dilution ratio of 1:4 (v/v), to have a concentration range of 3.8 nM to 62.5 μM. For derivatization, 30 μl of each supernatant from the samples or each standard solution was mixed with 30 μl of a mixed solution that contained predefined amounts of ¹³C or D-isotope-labeled analogues as internal standards for the 22 individual analytes, 60 μl of 50 mM dansyl chloride solution in acetonitrile, and 30 μl of borate buffer (pH 9.2). The mixtures were reacted at 40 °C for 45 min, and after reaction, each solution was diluted with 150 μl of water. Twenty microlitre aliquots were injected for UPLC-MRM/MS runs with positive-ion detection. The chromatographic separation was carried out on an Agilent Eclipse RRHD C18 column (2.1 mm I.D. x 150 mm, 1.8 μm) with 0.1% formic acid in water (A) and acetonitrile-isopropanol-formic acid (50:50:0.1, v/v/v) as the mobile phase for binary-solvent gradient elution. The elution gradient was 20% to 50% B in 5 min; 50% to 100% B in 10 min, followed by 4 min column equilibrium between injections. The flow rate was 0.3 ml/min and the column temperature was 50 °C. The concentrations of the metabolites in each sample were calculated from linearly-regressed calibration curves for individual compounds with internal calibration.

Study of apoptosis in cell cultures with Annexin V-FITC/Propidium Iodide staining

Cell apoptosis was assessed using an Annexin V-FITC/Propidium Iodide (PI) Apoptosis Detection Kit (Abcam). Briefly, the cells treated by 2-oxoadipic acid and quinolinic acid were washed and labelled with annexin V-FITC conjugate and PI solution at room

temperature for 15 min in the dark. Immunofluorescence images were collected using a Zeiss Axioimager Z1 fluorescence microscope equipped with Zeiss Apotome 2 (Zeiss, Germany). Acquired images were processed with ZEN (2012) software.

Supplementary figure 1: alignment of SLC25A21 against BtAAC1 using Clustal Omega

(<http://www.ebi.ac.uk/Tools/msa/clustalo/>)

CLUSTAL O(1.2.1) multiple sequence alignment

```
SLC25A21      MAKPEVSLVREASRQIVAGGSAGLVEICLMHPLDVVKTRFQIQRCA---TDPNSYKSLVD
BtAAC1        MSDQALSF----LKDFLAGGVAAAISKTAVAPIERVKLLQVQHASKQISAEKQYKGIID
               *: .  *:      :::*** *. .  :  *: : **  :*: : :  :  :. * . : : *
SLC25A21      SFRMIFQMEGLFGFYKILPPILAETPKRAVKFFTFEQYKLL-GYVSLSPA-LTFAI--
BtAAC1        CVVRIPKEQGFSLFWRGNLANVIRYFPTQALNFAFKDKYKQIFLGGVDRHKQFWRVYFAGN
               .. * : :*: :*: * *  :  * . : : *  :*: : : * * .      :
SLC25A21      ---AGLGSLTEAIVVNPFEVVKVGLQANRNTFAEQPSTVGYARQIIK-KEGWGLQGLNKG
BtAAC1        LASGGAAGATSLCFVYPLDFARTRLAADVKGAAQREFTGLGNCITKIFKSDGLRGLYQG
               :* .: * * .  . * * : : : . * * . * * . * *  : . * : * * : *
SLC25A21      LTATLGRHGVFNMVYFGFYNVKNMIPVVKDPIL-EFWRKFGIGLLSGTIASVINIPFDV
BtAAC1        FNVSVQGIIRAAAYFGVYDTAKGMLPDPKNVHIIVSWM---IAQTVTAVAGLVSYPFDT
               : . : :      : : . * * . * . * * * : :  *  * .      : * . : : * *
SLC25A21      AKSRIQGPQP-VPGEIKYRTCFKTMATVYQEEGILALYKGLLPKIMRLGPGGAVMLLVYE
BtAAC1        VRRRMMMQSGRKGADIMYGTVCWRKIAKDEGPKAFFKGAWSNVL-RGMGAFVLVLYD
               . : * :  .  . * *  . .  . : : * *  * : * *  : : * * * * . : : * : *
SLC25A21      YTYSWLQENW
BtAAC1        EIKKFV----
               . : :
```

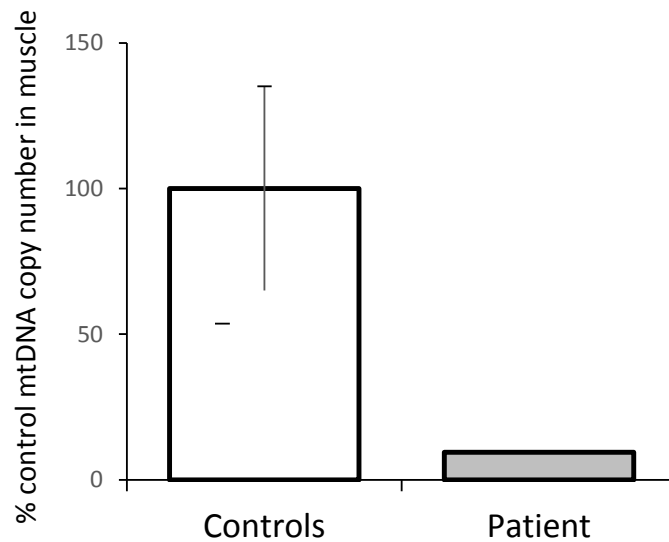
Supplementary figure 2: alignment of SLC25A21 against the N-terminal truncation Δ 2-4 using

Clustal Omega (<http://www.ebi.ac.uk/Tools/msa/clustalo/>)

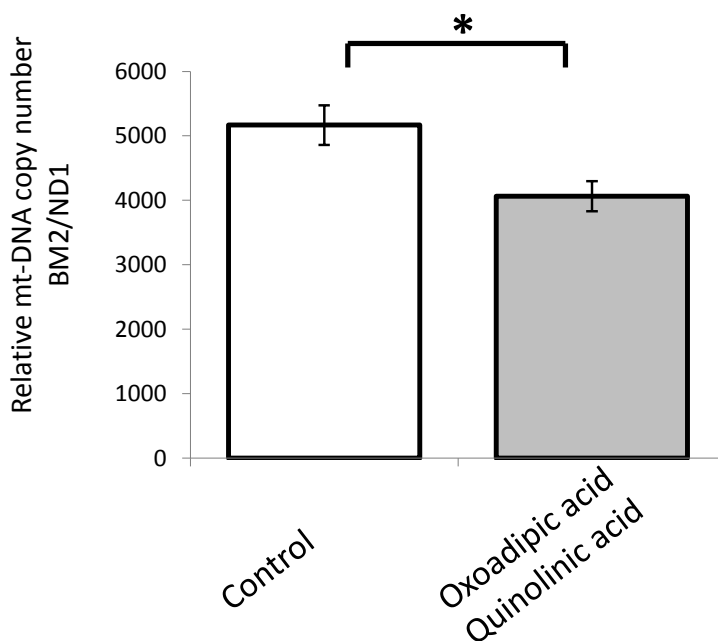
CLUSTAL O(1.2.1) multiple sequence alignment

```
SLC25A21      MAKPEVSLVREASRQIVAGGSAGLVEICLMHPLDVVKTRFQIQRCATDPNSYKSLVDSFR
Delta_2_4     ---MEVSLVREASRQIVAGGSAGLVEICLMHPLDVVKTRFQIQRCATDPNSYKSLVDSFR
               *****
SLC25A21      MIFQMEGLFGFYKILPPILAETPKRAVKFFTFEQYKLLGYVSLSPALTFIAGLGSL
Delta_2_4     MIFQMEGLFGFYKILPPILAETPKRAVKFFTFEQYKLLGYVSLSPALTFIAGLGSL
               *****
SLC25A21      TEAIVVNPFEVVKVGLQANRNTFAEQPSTVGYARQIIKKEGWGLQGLNKGLTATLGRHGV
Delta_2_4     TEAIVVNPFEVVKVGLQANRNTFAEQPSTVGYARQIIKKEGWGLQGLNKGLTATLGRHGV
               *****
SLC25A21      FNMVYFGFYNVKNMIPVVKDPILFWRKFGIGLLSGTIASVINIPFDVAKSRIQGPQPV
Delta_2_4     FNMVYFGFYNVKNMIPVVKDPILFWRKFGIGLLSGTIASVINIPFDVAKSRIQGPQPV
               *****
SLC25A21      PGEIKYRTCFKTMATVYQEEGILALYKGLLPKIMRLGPGGAVMLLVYEYYSWLQENW
Delta_2_4     PGEIKYRTCFKTMATVYQEEGILALYKGLLPKIMRLGPGGAVMLLVYEYYSWLQENW
               *****
```

Supplementary figure 3: Muscle mtDNA copy number was determined in the patient and compared to controls (n=25) as previously described¹, expressing the data as a % of mean control mtDNA copy number. Patient muscle revealed a significant mtDNA depletion (<10% of age-matched controls).



Supplementary figure 4: MtDNA copy number measurement after 5 days supplementation of 2-oxoadipate and quinolinic acid *in vitro* in SHSY-5Y cells showed slight, but significant reduction of mtDNA on paired t-test. The two-tailed P value equals 0.0369.



Reference:

1. Blakely, E. *et al.* Novel mutations in the *TK2* gene associated with fatal mitochondrial DNA depletion myopathy. *Neuromusc. Disord.* **18**, 557-560. doi: 10.1016/j.nmd.2008.04.014 (2008).